

Peer review status:

This is a non-peer-reviewed preprint submitted to EarthArXiv.

Artificial Intelligence-Based Joint Retrieval Algorithm for Land Surface Temperature, Emissivity, and Atmospheric Water Vapor

Liurui Xiao^{a,b,★}, Kebiao Mao^{b,*,★}, Chunshu Li^a, Jiancheng Shi^c, Sayed M. Bateni^{d,e}, Wang Dai^{a,b}

^a School of Electrical and Electronic-Engineering, Ningxia University, Yinchuan 750021, China.

^b State Key Laboratory of Efficient Utilization of Arid and Semi-arid Arable Land in Northern China, Institute of Agricultural Resources and Regional Planning, Chinese Academy of Agricultural Sciences, Beijing 100081, China.

^c National Space Science Center, Chinese Academy of Sciences, Beijing 100190, China. shijiancheng@nssc.ac.cn

^d Department of Civil and Environmental Engineering and Water Resources Research Center, University of Hawaii at Manoa, Honolulu, HI 96822, USA. smbateni@hawaii.edu

^e UNESCO-UNISA Africa Chair in Nanoscience and Nanotechnology College of Graduates Studies, University of South Africa, Muckleneuk Ridge, Pretoria, 392, South Africa

Correspondence to: Kebiao Mao (maokebiao@caas.cn)

★ These authors contributed equally to this work.

Preprint Declaration:

This is a non-peer-reviewed preprint submitted to EarthArXiv. The manuscript is currently under peer review at IEEE Transactions on Knowledge and Data Engineering. The content matches the version submitted to the journal.

Funding:

This research was supported by key Project of Natural Science Foundation of Ningxia Department of Science and Technology (No. 2024AC02032), Fengyun Satellite Application Pilot Program "Development and Application of Fengyun all-weather Land Surface Temperature Spatiotemporal Fusion Dataset" (FY-APP-2022.0205).

Declaration

The authors declare that they have no known competing financial interests or personal relationships that could have appeared to influence the work reported in this paper.

Acknowledgments

The MODIS thermal infrared data used in this study were provided by the National Aeronautics and Space Administration (NASA), and we extend our gratitude for their support. We also appreciate the Surface Radiation Budget Network (SURFRAD) ground observation data provided by the National Oceanic and Atmospheric Administration (NOAA), the AERONET ground observation data provided by NASA and the French National Center for Scientific Research (CNRS), and the ERA5 reanalysis data provided by the European Centre for Medium-Range Weather Forecasts (ECMWF). These high-quality datasets were crucial to the successful completion of this research.

Citation:

Liurui Xiao, Kebiao Mao, Chunshu Li, Jiancheng Shi, Sayed M. Bateni, Wang Dai, Artificial Intelligence-Based Joint Retrieval Algorithm for Land Surface Temperature, Emissivity, and Atmospheric Water Vapor, EarthArXiv, 2025,4.

Artificial Intelligence-Based Joint Retrieval Algorithm for Land Surface Temperature, Emissivity, and Atmospheric Water Vapor

Liurui Xiao^{a,b,*}, Kebiao Mao^{b,*,*}, Chunshu Li^a, Jiancheng Shi^c, Sayed M. Bateni^{d,e}, Wang Dai^{a,b}

^a School of Electrical and Electronic-Engineering, Ningxia University, Yinchuan 750021, China. Lichsh@nxu.edu.cn

^b State Key Laboratory of Efficient Utilization of Arid and Semi-arid Arable Land in Northern China, Institute of Agricultural Resources and Regional Planning, Chinese Academy of Agricultural Sciences, Beijing 100081, China.

^c National Space Science Center, Chinese Academy of Sciences, Beijing 100190, China. shijiancheng@nssc.ac.cn

^d Department of Civil and Environmental Engineering and Water Resources Research Center, University of Hawaii at Manoa, Honolulu, HI 96822, USA. smbateni@hawaii.edu

^e UNESCO-UNISA Africa Chair in Nanoscience and Nanotechnology College of Graduates Studies, University of South Africa, Muckleneuk Ridge, Pretoria, 392, South Africa

Correspondence to: Kebiao Mao (maokebiao@caas.cn)

★ These authors contributed equally to this work.

Abstract: The thermal infrared remote sensing parameters exhibit interdependent and mutually constrained relationships, which conventional methods fail to fully exploit for improving the overall retrieval accuracy across different parameters. To address this challenge, this study proposes an artificial intelligence-based method for jointly retrieving land surface temperature (LST), emissivity (LSE), and atmospheric water vapor content (WVC) from thermal infrared remote sensing data, achieving an organic integration of physical mechanism-based and statistical approaches. The model is initially applied to retrieve LST and LSE, which are then utilized as prior knowledge for cross-iterative WVC retrieval. The simulation validation results demonstrate that the four-band combination scheme for LST retrieval achieved optimal theoretical accuracy, with a mean absolute error (MAE) of 0.51 K and root mean square error (RMSE) of 0.69 K. The retrieval RMSE values for both LSE31 and LSE32 remained below 0.01. Incorporating LST and LSE information with the four thermal infrared bands further enhanced WVC retrieval stability, yielding an MAE of 0.05 g/cm² and RMSE of 0.08 g/cm². Finally, cross-validation and ground-based verification using the optimal band combination confirmed the overall reliability of the retrieval results. The retrieval errors for all parameters were reduced during nighttime due to decreased solar irradiation interference. Overall, the proposed joint retrieval method improved both accuracy and stability for all parameters, overcoming the limitations of conventional techniques and enhancing overall retrieval performance.

Keywords: Artificial intelligence; land surface temperature; emissivity; atmospheric water vapor; deep learning

1. Introduction

Land surface temperature (LST) and land surface emissivity (LSE) as well as atmospheric water vapor content (WVC) are key parameters for the study of the earth's energy balance and water cycle, which have a profound impact on agricultural production, climate change and water resources management (Moisa et al., 2022; Mikhaylov et al., 2020; Anderson et al., 2003; Reynolds et al., 2008). The different parameters are interrelated, with LST directly reflecting the surface's ability to absorb solar energy and its thermal response to the environment, while LSE determines the efficiency with which the surface emits thermal radiation into the atmosphere (Wan et al., 2004; Snyder et al., 1998). Additionally, WVC in the atmosphere not only affects the transmission of solar radiation but also can influence the measurement of LST and LSE (Padmanabhan et al., 2009), because WVC can absorb and re-radiate the thermal energy emitted by the surface. Accurately retrieving these variables has long been a significant challenge in agriculture. Precise measurement of these parameters is essential for informed agricultural decision-making, crop yield optimization, and effective resource management. However, traditional algorithms often struggle due to the complexity of the models and the uncertainty of input data. With the rapid advancement of AI, it is increasingly being integrated into agriculture (Akkem et al., 2023). AI-based algorithms can process large volumes of complex data, automatically identifying patterns and correlations, which allows for more accurate and real-time parameter estimation. By leveraging these advanced technologies, we can enhance the accuracy of joint retrievals for LST, LSE, and WVC.

In recent decades, many scholars have conducted in-depth research on the retrieval of individual parameters, and have developed various quantitative retrieval algorithms based on thermal infrared (TIR) remote sensing data, aiming for higher accuracy (Seguin et al., 1999). In the field of LST retrieval using TIR remote sensing, algorithms based on different band configurations are generally categorized into single-channel, split-window, and multi-channel approaches. The single-channel method estimates LST by formulating a radiative transfer equation using data from one thermal infrared channel within the atmospheric window, with known LSE, WVC, and atmospheric mean radiative temperature as prior knowledge. The most representative is the single-window algorithm proposed by Qin et al. (2001a) for TM6. The input parameters for the algorithm include brightness temperatures (BTs), along with known atmospheric transmittance, surface emissivity, and mean atmospheric temperature as prior knowledge. Jiménez-Muñoz and Sobrino (2003) proposed a generalized single-channel algorithm for calculating LST under known LSE and WVC conditions. Cristobal et al. (2009) further improved this method by incorporating near-surface air temperature (NSAT) into the generalized single-channel algorithm, enhancing the accuracy of atmospheric parameter estimation. While these methods improve the accuracy of LST retrieval in single-channel algorithms to some extent, they also require multiple prior parameters, which increases the complexity of the algorithm. The split-window algorithm establishes a radiative transfer equation to retrieve LST by utilizing the differences between two TIR bands. This method requires careful consideration of the effects of emissivity and atmospheric conditions (McMillin and Larry, 1975; Price, 1984; Becker and Li, 1990). For instance, Qin et al. (2001b) derived a Split-Window (SW) algorithm for retrieving LST from Advanced Very High-Resolution Radiometer (AVHRR) data. This algorithm primarily focuses on atmospheric transmittance and LSE, facilitating the broader application of the SW algorithm to other thermal infrared datasets. Wan and Dozier (1996) proposed

a general split window algorithm (GSW) by constructing a lookup table of the coefficients of the local split window algorithm considering the influence of three factors: LSE, water vapor content and observation skylight Angle. Wan (2014) added a quadratic term on the basis of GSW algorithm to improve the retrieval accuracy of LST on bare land surface types.

The multi-channel algorithm primarily uses a combination of at least three TIR bands to establish a set of radiative transfer equations, simultaneously retrieving LST and LSE. Such as the Temperature and Emissivity Separation (TES) algorithm mainly uses radiance brightness temperatures (BTs) obtained from different spectral channels to decouple and simultaneously estimate these two parameters. The TES algorithm, proposed by Gillespie et al. (1998), has been successfully applied to ASTER imagery. Nie et al. (2021) validated the applicability of the TES algorithm to different sensor data by retrieving LST and LSE from nighttime mid-infrared and thermal infrared Sentinel-3 images. The physics-based day/night algorithm improves the accuracy of retrievals by combining daytime and nighttime radiance observations and using a physical model to retrieve temperature and emissivity (Wan and Li, 1997, 2008). The stepwise retrieval method uses a step-by-step optimization approach to gradually correct inaccuracies in LSE, thereby enhancing the accuracy of LST retrievals (Lan et al., 2021; Yin et al., 2020). Furthermore, with the advancement of AI technology, Mao et al. (2007) proposed an algorithm that utilizes a combined radiative transfer model and neural network algorithm to simultaneously retrieve LST and LSE, which further improves the retrieval accuracy compared to other methods.

There are two representative algorithms for retrieving WVC based on thermal infrared remote sensing, the first is the traditional multi-band infrared statistical regression method. The basic process involves selecting BTs from multiple infrared bands as independent variables, using an atmospheric radiative transfer model to simulate radiance values under different water vapor content, and establishing a regression model through statistical regression analysis. Seemann et al. (2003) developed an operational method for retrieving atmospheric temperature, water vapor, and ozone using MODIS infrared radiance data, demonstrating the practical effectiveness of the multi-band infrared data regression method. Tu and Lu (2020) studied the relative importance of water vapor and air temperature in the interannual variability of seasonal precipitation by comparing physical and statistical methods. The second method is the split-window approach, which is achieved by constructing a fitted relationship or empirical equation between water vapor content (WVC) and atmospheric transmittance or the ratio of transmittances. Dalu (1986) first proposed the atmospheric water vapor split-window algorithm, establishing a linear relationship between WVC and the difference in BTs from AVHRR thermal infrared channels. Sobrino et al. (1999) proposed the Split-Window Covariance-Variance Ratio (SWCVR) algorithm and used AVHRR data to calculate WVC over the Iberian Peninsula, achieving an accuracy of 0.5 g/cm². In addition, various neural networks have been applied in recent years to model the complex nonlinear relationships of WVC (Huang et al., 2021; Toporov et al., 2020; Zhang and Yao, 2021). These advancements have significantly enhanced the accuracy and efficiency of WVC retrieval, demonstrating their robust potential and adaptability.

In summary, despite significant advancements in the retrieval of individual parameters, these methods are limited by their failure to fully exploit the potential information among multiple parameters, thereby affecting the overall accuracy of the retrievals. In recent years, the rapid development of deep learning technology with the ability to fit complex functions and self-learning

has shown great potential in accurately approximating complex nonlinear relationships in remote sensing retrieval, which can deeply mine and utilize the interrelations between parameters (Li et al., 2022; Mao et al., 2011; Mao et al., 2023a). Therefore, to further improve the retrieval accuracy of thermal infrared LST, LSE, and WVC, we propose a multi-parameter joint retrieval method framework based on AI. Firstly, the physical retrieval method is constructed by deducing the physical radiation transfer equation. Then a generalized statistical method is constructed based on the physical method. Then, the deep learning training and testing database is constructed by the representative solutions of physical methods and statistical methods to complete the deep learning coupling. LST and LSE are retrieved by AI, and then they are used as the prior knowledge of WVC retrieval. Finally, cross-iteration is performed until the highest accuracy is achieved.

2. Methodology

To fully utilize the potential information among LST, LSE, and WVC, and to overcome the ill-posed problems present in traditional methods, we employ AI techniques to explore the hidden patterns and interrelationships among the parameters coupled in the thermal radiative transfer equation, thereby improving the overall accuracy of parameter retrieval. This study utilizes deep learning to couple physical and statistical methods for the joint retrieval of LST, LSE, and WVC from thermal infrared remote sensing data. The framework of the retrieval method is illustrated in **Fig. 1**. In terms of physical methods, we perform physical logical reasoning on the retrieval mechanism of the main parameters based on the radiative transfer equation, analyzing the relationships between BT and LST, LSE, and WVC. This involves determining the causal relationships between input and output parameters in the deep learning process, ensuring that the equations between input and output parameters can be theoretically solved (Mao et al., 2023b). The forward model MODTRAN is then used to simulate the representative solution of the physical method. Based on this, we further establish generalized statistical methods to use multi-source data to obtain reliable representative solutions of statistical methods as a supplement to the solutions of physical methods, this is because the simulated data only represent clean pixels, while most images contain mixed pixels. The solution set of physical and statistical methods constitutes the training and testing database of deep learning, which enables deep learning to couple physical and statistical methods.

During the retrieval process, it is essential to systematically evaluate the impact of different band combinations on the accuracy of LST, LSE, and WVC retrieval to identify the most effective combination. This process utilizes large-scale remote sensing datasets and leverages artificial intelligence techniques, including deep learning neural networks (DL-NN). Deep learning models are capable of extracting key features of LST and LSE from complex data. The retrieved LST and LSE are subsequently used as prior knowledge for WVC retrieval. A cross-iteration strategy is employed to optimize the computation of WVC, reducing uncertainties in the retrieval process and improving accuracy. Through cross-iteration, our model can progressively refine the retrieved WVC values, bringing them closer to the actual conditions. Finally, to validate the effectiveness of this method, we compared the retrieved parameters with various data products, including in-situ ground measurements and high-precision MODIS LST products. Artificial intelligence technology, particularly the use of deep learning to couple traditional physical understanding with modern statistical analysis, continually optimizes computations to approach the optimal solution, thus

providing more accurate and stable outputs for the joint retrieval of thermal infrared remote sensing parameters.

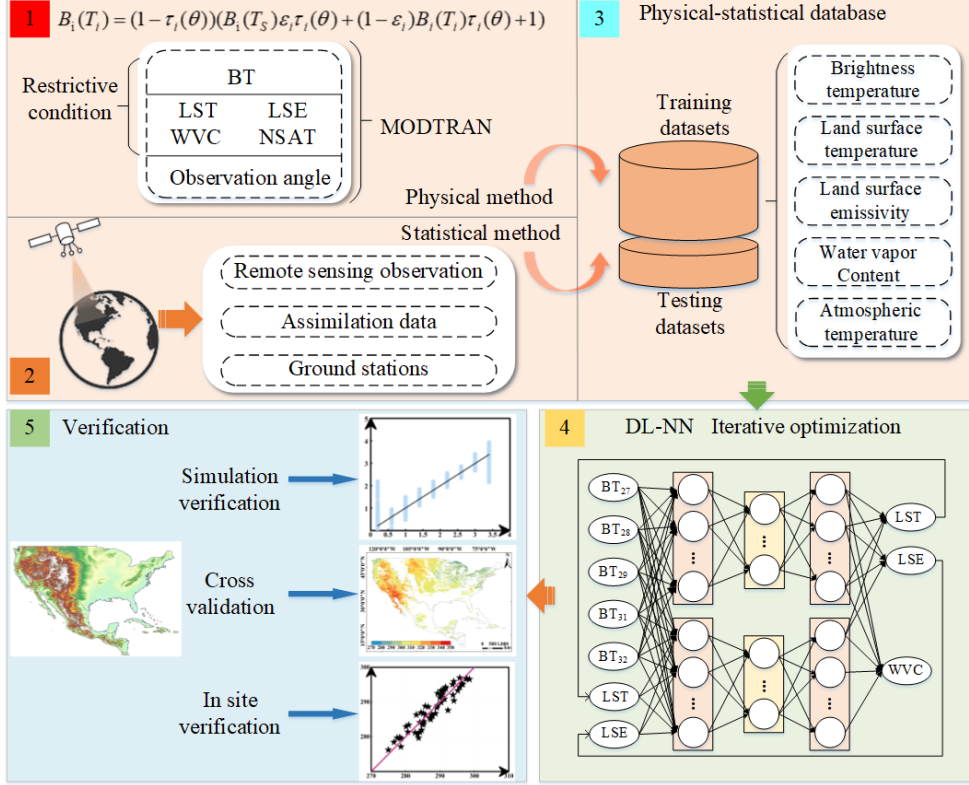


Fig. 1. Deep learning retrieval algorithm framework coupled with physical-statistical methods

3. Methods and Materials

3.1 Physical logic reasoning

The joint retrieval algorithm for LST, LSE, and WVC is based on a radiative transfer (RT) process. As illustrated in Fig.2, the RT process simulates the path of thermal radiation emitted from the surface as it travels through the atmosphere and is ultimately detected by satellite sensors. This process accounts for how both surface characteristics and atmospheric conditions influence the radiation signal transmitted from the surface to the satellite. Thermal radiation emitted from the surface is influenced by various factors as it passes through the atmosphere to reach satellite sensors. These factors primarily include surface type (e.g. soil, vegetation, water, and rocks), soil moisture, LST, WVC, and near-surface air temperature (NSAT) (Wan and Li, 1997). Consequently, the radiance detected by satellites at the top of the atmosphere is typically a combined result of LSE, LST, and atmospheric radiation. The radiative process comprises three main components: the surface-emitted radiation that reaches the sensor after atmospheric absorption, the upward atmospheric radiation, and the downward atmospheric radiation reflected by the surface. In cloud-free, clear-sky conditions with local thermal equilibrium, the radiance observed by the sensor at a given angle can be expressed by Eq. (1).

$$B_i(T_i) = \epsilon_i B_i(T_s)\tau_i(\theta) + (1 - \epsilon_i)\tau_i(\theta)R_i^\downarrow(\theta) + R_i^\uparrow(\theta) \quad (1)$$

Where T_s is the LST, and T_i is the BT (K) in channel i , $\tau_i(\theta)$ is the atmospheric transmittance in channel i at an observation angle θ (zenith angle from nadir), ε_i is the LSE, $B_i(T_i)$ is the thermal radiance received by the sensor in band i ($W \cdot m^{-2} sr^{-1} \mu m^{-1}$), $R_i^\downarrow(\theta)$ and $R_i^\uparrow(\theta)$ are the downward and upward atmospheric thermal radiance in band i , respectively. The radiance emitted by the surface and the atmospheric downward radiance reflected by the surface are attenuated by atmospheric absorption as they travel to the sensor.

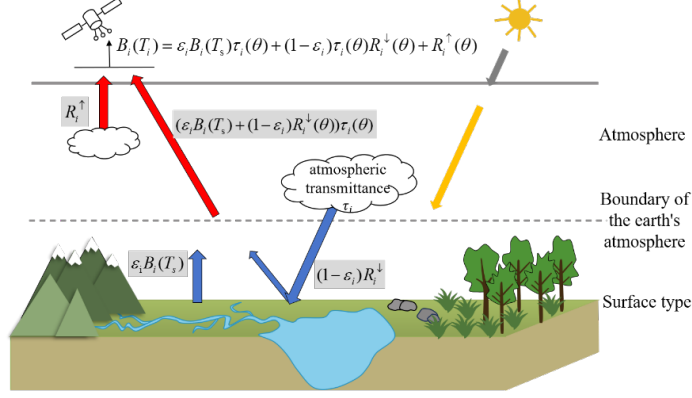


Fig. 2. Atmospheric radiative transfer process

For a blackbody, the energy absorbed is equal to the energy emitted, and the emissivity is 1. Its radiance is directly related to temperature and wavelength, which can be expressed using the Planck function, as shown in Eq. (2).

$$B_i(T_i) = \frac{C_1}{\lambda^5 (e^{\frac{C_2}{\lambda T_i}} - 1)} \quad (2)$$

Where $C_1 = 2c^2 h = 1.191 \times 10^8 (W \cdot m^{-4} sr^{-1} \mu m^{-2})$, $C_2 = \frac{ch}{k} = 1.439 \times 10^4 (\mu m \cdot K)$. Where c is the speed of light, with a value of $3 \times 10^8 (m \cdot s^{-1})$, h is the Planck constant, with a value of $6.63 \times 10^{-34} (J \cdot s)$, and k is the Boltzmann constant, with a value of $1.38 \times 10^{-23} (J \cdot K^{-1})$. Assuming the sensor measures the thermal radiance of a specific band i , the radiance can be converted to brightness temperature using Planck's law, as shown in Eq. (3).

$$T_i = \frac{C_2}{\lambda \ln(1 + \frac{C_1}{\lambda B_i(T_i)})} \quad (3)$$

According to Franc and Cracknell (1994), upward and downward atmospheric radiation can be expressed as Eq. (4) and Eq. (5).

$$R_i^\uparrow(\theta) = \int_0^Z B_i(T_z) \frac{\partial \tau_i(\theta, z, Z)}{\partial z} dz \quad (4)$$

$$R_i^\downarrow(\theta) = 2 \int_0^{\frac{\pi}{2}} \int_h^0 B_i(T_z) \frac{\partial \tau_i(\theta', z, 0)}{\partial z} \cos \theta' \sin \theta' dz d\theta' \quad (5)$$

Where T_z is the atmospheric temperature at the height z , Z is the sensor height, θ is the upward direction of atmospheric radiation, $\tau_i'(\theta, z, Z)$ represents the upward atmospheric transmittance from the height z to the sensor, θ' represents the downward direction of atmospheric radiation, h represents the atmospheric height, $\tau_i'(\theta', z, 0)$ represents the descending atmospheric transmittance from height z to the surface. Qin et al. (2001b) used the mean value theorem to deal with the ascending and descending atmospheric radiation, so we got Eq. (6) and Eq. (7).

$$R_i^\uparrow(\theta) = (1 - \tau_i(\theta))B_i(T_a) \quad (6)$$

$$R_i^\downarrow(\theta) = (1 - \tau_i(\theta))B_i(T_a^\downarrow) \quad (7)$$

In the equation, T_a represents the effective mean atmospheric temperature, and T_a^\downarrow denotes the downward effective mean atmospheric temperature. $B_i(T_a)$ and $B_i(T_a^\downarrow)$ denote the effective mean atmospheric radiation in band i corresponding to T_a and T_a^\downarrow . Qin et al. (2001b) concluded through sensitivity analysis that replacing T_a^\downarrow with T_a in the equation does not result in any significant impact on the calculation results. Therefore, the equation can be described as Eq. (8).

$$B_i(T_i) = \varepsilon_i \tau_i(\theta) B_i(T_s) + (1 - \tau_i(\theta))(1 - \varepsilon_i) \tau_i(\theta) B_i(T_a) + (1 - \tau_i(\theta)) B_i(T_a) \quad (8)$$

From this, it can be seen that each band's radiative transfer equation contains four unknowns, if there are N bands, there will be $2N+2$ unknowns (the transmittance and emissivity for each of the N bands, along with the LST and the mean atmospheric temperature), which is a typical pathological problem. So, we have to reduce the variables in the radiative transfer equation according to the correlation between the geophysical variables.

LSE is an intrinsic physical property of ground objects, reflecting their ability to absorb and emit radiative energy. It is influenced by factors such as surface type, roughness, and water content, and its value varies depending on the wavelength and observation angle. If each type of ground is known, the LSE for each band can be determined. Thus, all unknown LSEs in different bands can be unified into a single unknown parameter (surface type) like Eq. (9).

$$\varepsilon_i = F(\text{surface_type}) \quad (9)$$

In addition, the atmospheric transmittance is mainly affected by the WVC and other gases (g), whose transmittance can be expressed as Eq. (10).

$$\tau_i = F(WVC, g) \quad (10)$$

The mean atmospheric temperature is closely related to the WVC and NSAT. However, current methods find it challenging to calculate accurately, as it is typically derived from the weighted average of water vapor content and temperature across different atmospheric layers. There is a strong linear relationship between the effective mean atmospheric temperature and near-surface air temperature, which can be expressed by Eq. (11).

$$T_a = A + BT_n \quad (11)$$

Where T_n represents NSAT, A is a constant, and B is a coefficient. Some researchers have found that within a certain geographical range, there is a strong linear relationship between the effective mean atmospheric temperature T_a and the satellite-derived brightness temperature T_i . the effective mean atmospheric temperature. The expression can be depicted as Eq. (12) (Mao et al., 2007; Wang et al., 2021).

$$T_a \approx A' + B'T_i \quad (12)$$

In the equation, A' is a constant, B' is a coefficient. These coefficients vary depending on the region and season.

From the above derivation and analysis, it can be concluded that the radiative transfer equation can be simplified to four unknowns (WVC, LST, surface type, and effective mean atmospheric temperature). To obtain a unique solution to the equation without prior knowledge, at least four thermal infrared window bands are required to construct a system of equations (number of equations

\geq number of unknowns). Suppose deep learning is used to optimize the calculation method. In that case, the equation can be simplified to three unknowns (WVC, LST, and surface type) based on the linear relationship between effective mean atmospheric temperature and BTs. This means that at least three bands can construct the system of equations, though the accuracy might be affected.

Overall, there is a strong constraint relationship between LST, LSE, WVC, NSAT, and BT. However, this constraint relationship cannot be strictly defined, which introduces uncertainties in the calculation process for traditional methods. By utilizing AI techniques for joint retrieval and cross-iteration, the retrieval accuracy can be improved.

3.2 Generalized statistical methods

Physical methods can obtain representative solutions through high-precision model simulation, but due to the limitations of forward modeling models in reality, physical models cannot simulate all cases, so we construct generalized statistical methods to make up for this defect. The representative solution of this generalized statistical method is mainly obtained through multi-source data collection, which is inconsistent with the traditional statistical method. During data collection, the statistical and physical methods should align in terms of the position and number of bands used, while also satisfying the fundamental requirements of the physical method. To improve the method's applicability, prior knowledge such as LST and LSE must be incorporated for WVC retrieval, enhancing both the stability and accuracy of the process. According to the derivation of the above physical method, the statistical method needs at least four TIR bands to achieve high accuracy, and the statistical method can be depicted as Eq. (13).

$$LST / LSE / WVC = \sum_{i=1}^n \prod f(T_i) + b \quad (13)$$

Where T_i is the TIR band, $f(T_i)$ is the correlation generalization function, and b is the constant. To improve the accuracy and versatility of the retrieval, high-precision statistical sample data from multiple channels were collected. The collection of these data provides the basis for deep learning methods to couple generalized statistical methods. In this way, deep learning is used to achieve the retrieval goal in a data-driven way.

3.3 Deep learning coupled physics and statistical methods

Thermal infrared remote sensing parameters are retrieved by constructing a system of radiative transfer equations, which theoretically allows for a solution. However, the inclusion of the Planck equation complicates practical solutions. Leveraging the universal approximation capability of fully connected neural networks (FNNs) (Mao et al., 2008), we generated a dataset from physical and statistical methods, which was then randomly divided into training and testing sets at a ratio of 7:3. By integrating deep learning with physical and statistical methods, we effectively approximated the solution curves of the equations, thereby simplifying the inversion process and improving accuracy.

FCNNs are a widely used feedforward neural network training algorithm. By combining multiple layers and nonlinear activation functions, FCNNs can leverage their nonlinear fitting capabilities to learn complex relationships between inputs and outputs (Hornik et al., 1989). Through training on large-scale data, FCNNs can identify important patterns and features in the data, automatically learning feature representations, thereby better understanding the mapping between inputs and outputs. Additionally, FCNNs employ end-to-end learning, optimizing the entire process from input to output. This end-to-end learning approach simplifies the modeling process, making neural

networks more flexible and adaptable to various retrieval challenges, while significantly enhancing the accuracy and speed of atmospheric remote sensing retrievals. As illustrated in **Fig. 3**, a typical FCNN comprises an input layer, an output layer, and multiple hidden layers (Jha et al., 2019). The number of neurons in each layer is determined by the initial parameter configuration. Activation functions are essential in neural networks, as they introduce nonlinearity, improve model robustness, and help mitigate the vanishing gradient problem. The weights and biases of each neuron are expressed in Eq. (14).

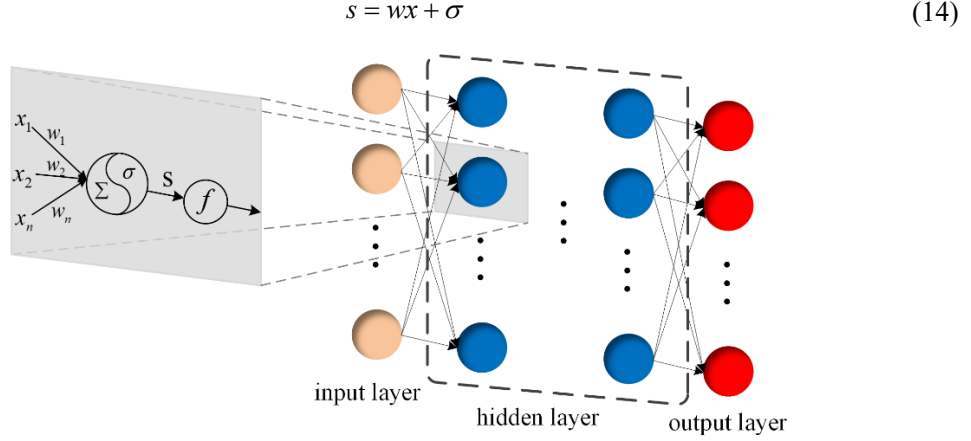


Fig. 3. Deep learning neural network model

There are various choices for nonlinear activation functions, each with specific advantages and suitable scenarios. Common and suitable activation functions can improve the performance and expressiveness of the model, such as the Sigmoid function Eq. (15).

$$f(x) = \frac{1}{1 + e^{-s}} = \frac{1}{1 + e^{-(wx + \sigma)}} \quad (15)$$

The resulting activation functions as the input for subsequent neurons or as the network's output. A neuron's input can either be the original input x of the entire network or the output from a preceding neuron. The performance of a neural network largely depends on its architecture and training data, requiring repeated experiments to optimize the number of hidden layers and nodes to improve retrieval accuracy.

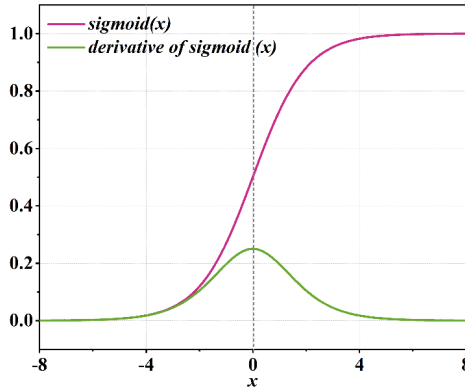


Fig. 4. Sigmoid function and its derivatives

3.4 Materials

3.4.1 Remote sensing data

MODIS (Moderate Resolution Imaging Spectroradiometer) is a hyperspectral radiometer onboard the Terra and Aqua satellites (Salomonson et al., 1989). It features 36 spectral bands covering the visible, near-infrared, shortwave infrared, and mid-infrared regions of the electromagnetic spectrum. The thermal infrared bands of MODIS exhibit high calibration accuracy and can be used to retrieve various meteorological and environmental parameters, including surface reflectance, temperature, atmospheric temperature, water vapor content, clouds, and aerosols.

The study selected MODIS TIR bands 27/28/29/31/32 for simulation and analysis due to their spectral characteristics aligning with the inversion objectives. Band 27 (6.72 μm) is located within the strong water vapor absorption region, while bands 28 (7.33 μm) and 29 (8.55 μm) are near the edge of the water vapor absorption zone, making them suitable for retrieving LST and WVC. Bands 31 (11.03 μm) and 32 (12.02 μm) lie within the atmospheric window, offering high accuracy and reliability for LST retrieval. LST, LSE, and WVC products from the MODIS sensor are well-established and extensively validated (Frantz et al., 2019; Wang et al., 2020), making them a reliable source for simultaneous high-precision LST and LSE data. The spectral response functions of the MODIS bands are shown in Fig. 5.

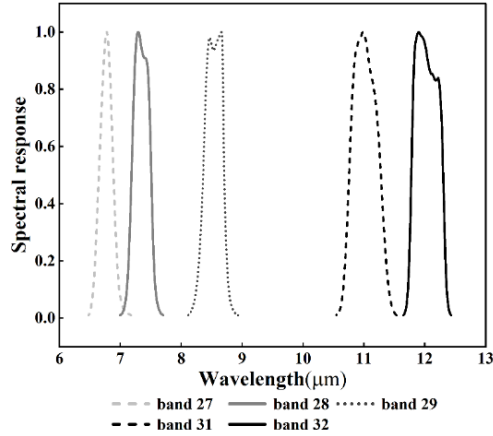


Fig. 5. MODIS band 27/28/29/31/32 spectral response function.

This study utilized various MODIS products, including MYD11_L2 and MYD05, to support the retrieval and analysis of LST, LSE, and WVC. These products have been rigorously validated (Wan, 2014; Gao et al., 2003) and offer high accuracy and global coverage, providing reliable data support for training deep learning models. In this study, we employed quality control (QC) data to filter high-quality pixels, minimizing the impact of cloud contamination. Data from August 2020 was collected as training data (363,800 sets) and test data (109,140 sets) for the neural network model. To further validate the model's generalization capability and reliability, independent MODIS data from August 2021 were used for validation analysis.

3.4.2 Simulated data

MODTRAN was utilized to generate high-precision simulated data, addressing the limitations in quantity and quality of actual measurements. Through MODTRAN simulations, we were able to precisely control input parameters, avoiding uncertainties inherent in real-world measurements, while ensuring consistency in key physical parameters such as spectral emissivity and water vapor content across different bands. This provided a reliable training foundation for the model. Specifically, the study focused on MODIS thermal infrared bands 27, 28, 29, 31, and 32, simulating

diverse surface characteristics by configuring various land cover types, atmospheric conditions, and observation geometries to comprehensively capture the diversity of real-world remote sensing scenarios. Additionally, different weather patterns were incorporated to further simulate complex atmospheric environments. Ultimately, the training data (126,800 sets) and test data (59,400 sets) in this simulation dataset not only cover a wide range of surface and atmospheric conditions, but also ensure intrinsic consistency between physical parameters, providing high-quality and diverse training samples for deep learning models. This significantly enhances the model's generalization capability and retrieval accuracy in practical applications. The specific parameter settings for MODTRAN are shown in **Table 1**.

Table 1. MODTRAN set specific parameters

Parameters	Intervals	Range
LSE	-	0.96~1.00
LST	3K	281~323
WVC	0.4g/cm ²	0.2~3.4
Observation Angle	3°	0~65°

3.4.3 Ground observation data

The Surface Radiation Budget Network (SURFRAD), established in 1993, aims to support climate research through accurate, continuous, and long-term measurements of the surface radiation budget across the United States (Ndossi and Avdan, 2016). As SURFRAD stations provide unique in-situ LST data in rural areas, many researchers have utilized these observations to validate satellite-based LST retrievals. The data is accessible via NOAA's official website (<https://www.esrl.noaa.gov/gmd/grad/surfrad/>). This study selects observational data from stations representing different land cover types.

The ground-based observational data used for WVC retrieval in this study are the rigorously quality-controlled Level 2.0 data provided by Aerosol Robotic Network (AERONET) stations, obtained from the official website (<https://aeronet.gsfc.nasa.gov/>). AERONET stations are globally distributed and conduct continuous measurements using standardized sun photometers. However, since sun photometers operate only during daylight, this study focuses on validating WVC under daytime conditions using observations from these stations.

Additionally, the acquired ground-based observational data undergo interpolation and rigorous quality control, including the removal of outliers and missing values, to ensure effective spatiotemporal consistency with satellite remote sensing products.

3.4.4 ERA5

ERA5-Land is generated by assimilating observational data into the Integrated Forecasting System of the European Centre for Medium-Range Weather Forecasts (ECMWF). It integrates satellite observations, ground-based measurements, and numerical models to produce high-quality reanalysis data, which has been validated across numerous research domains (Bai et al., 2021; Zhang et al., 2019). The data is publicly accessible through the Copernicus Climate Data Store (CDS) platform of ECMWF. This study utilizes the LST and WVC data from the hourly ERA5-Land

dataset as reference for calibration. Only when the accuracy of different product data is consistent is the data used for training and testing in deep learning models.

3.5 Evaluation index

To evaluate the accuracy of the constructed joint retrieval algorithm, a linear regression analysis is conducted between the true values and the retrieved parameter values. We selected four statistical values that reflect the true error situation of the retrieval results: Mean Absolute Error (MAE), Root Mean Square Error (RMSE), Bias, and the coefficient of determination (R^2).

MAE is a widely used statistical indicator for evaluating model efficiency. RMSE measures the deviation between the retrieved results and the true values. The coefficient of determination (R^2) assesses the goodness of fit of the regression model. The calculation formulas are shown below, where x represents the retrieved values, and y represents the true values.

$$MAE = \frac{1}{n} \sum_{i=1}^n |x_i - y_i| \quad (16)$$

$$RMSE = \frac{1}{n} \sqrt{\sum_{i=1}^n (x_i - y_i)^2} \quad (17)$$

$$R^2 = \left(\frac{\sum_{i=1}^n (x_i - \bar{x})(y_i - \bar{y})}{\sqrt{\sum_{i=1}^n (x_i - \bar{x})^2} \sqrt{\sum_{i=1}^n (y_i - \bar{y})^2}} \right)^2 \quad (18)$$

4. Results and Validation

4.1 Verification and analysis of theoretical accuracy

4.1.1 LST and LSE

Simulated data was used to assess and discuss the retrieval accuracy of LST, LSE, and WVC across various band combinations, and the theoretical accuracy was validated. For LST retrieval, three different band combinations were tested, with the results summarized in **Table 2-Table 4**. **Table 2** presents the error statistics for LST retrieval using bands 29, 31, and 32. The highest retrieval accuracy was achieved with a network configuration of 7 hidden layers and 600 nodes per layer, resulting in an MAE of 1.15K and an RMSE of 1.55K. As shown in **Table 3**, using bands 28, 29, 31, and 32 for LST retrieval achieved the highest accuracy with 8 hidden layers and 700 nodes per layer, resulting in an MAE of 0.51K and an RMSE of 0.69K. Incorporating band 28 significantly improved retrieval accuracy, reducing RMSE by 0.86K. Since band 28 is within the water vapor absorption range and is highly sensitive to WVC, it better corrects the influence of WVC on TIR bands, thereby enhancing LST retrieval accuracy. **Table 4** summarizes the retrieval errors for the 27-28-29-31-32 band combination. It can be seen from the table that the highest retrieval accuracy is achieved when the number of hidden layers is 6 and each layer has 800 hidden nodes (MAE=0.53 K, RMSE=0.75 K). The experimental results demonstrate that the inclusion of water vapor absorption bands can indeed effectively enhance the retrieval accuracy of atmospheric water vapor content parameters. However, MODIS band 27, as a deep water vapor absorption channel, exhibits low surface transmittance and thus contributes limitedly to directly improving land surface temperature (LST) retrieval accuracy. Therefore, it can be concluded that water vapor channels with moderate absorption intensity are more conducive to enhancing LST retrieval accuracy than strong absorption channels.

Table 2. Band 29, 31,32 combined retrieval LST error.

Layer \ Node	500		600		700		800		900	
	MAE	RMSE	MAE	RMSE	MAE	RMSE	MAE	RMSE	MAE	RMSE
6	1.17	1.61	1.18	1.58	1.17	1.57	1.16	1.57	1.17	1.58
7	1.18	1.70	1.15	1.55	1.18	1.59	1.15	1.57	1.17	1.59
8	1.18	1.62	1.19	1.60	1.18	1.59	1.20	1.65	1.23	1.69
9	1.19	1.59	1.18	1.60	1.20	1.63	1.20	1.64	1.21	1.72
10	1.20	1.61	1.17	1.71	1.21	1.64	1.21	1.64	1.22	1.63

Table 3. Band 28,29,31,32 combined retrieval LST error.

Layer \ Node	500		600		700		800		900	
	MAE	RMSE	MAE	RMSE	MAE	RMSE	MAE	RMSE	MAE	RMSE
6	0.55	0.76	0.55	0.74	0.55	0.81	0.53	0.74	0.54	0.75
7	0.54	0.72	0.52	0.73	0.56	0.76	0.53	0.75	0.55	0.78
8	0.52	0.71	0.54	0.79	0.51	0.69	0.54	1.26	0.52	0.72
9	0.56	0.75	0.57	0.93	0.53	1.37	0.54	0.78	0.52	0.71
10	0.57	0.77	0.53	0.73	0.54	0.79	0.54	1.42	0.55	0.78

Table 4. Band 27,28,29,31,32 combined retrieval LST error.

Layer \ Node	500		600		700		800		900	
	MAE	RMSE	MAE	RMSE	MAE	RMSE	MAE	RMSE	MAE	RMSE
6	0.75	1.68	0.55	1.15	0.69	1.68	0.53	0.75	0.90	3.69
7	0.69	1.42	0.92	3.21	0.68	1.83	0.57	1.13	0.55	0.97
8	0.63	1.43	0.76	2.07	0.71	2.51	0.71	1.68	0.70	2.34
9	0.58	1.23	0.61	1.29	0.83	2.99	0.74	2.70	0.66	1.51
10	0.82	2.08	0.57	1.20	0.55	1.04	0.84	2.83	0.64	1.51

Additionally, we conducted a statistical comparison analysis of the top three datasets in terms of accuracy from **Table 2-Table 4** (as shown in **Fig. 6**). **Fig. 6(a)(b)(c)** clearly demonstrates that including water vapor absorption bands significantly improves the accuracy of LST retrieval. Moreover, using a combination of four TIR bands results in a notable reduction in outliers and more stable retrieval results. In summary, to achieve a LST retrieval accuracy within 1 K, at least four TIR bands are required. This analysis validates the feasibility of our previous physical logic analysis. Additionally, while theoretical analysis suggests that multi-band combinations can improve retrieval accuracy, in practical applications, careful consideration of band selection and combination is necessary to avoid introducing excessive uncertainty and redundant information, ultimately enhancing the effectiveness of LST retrieval.

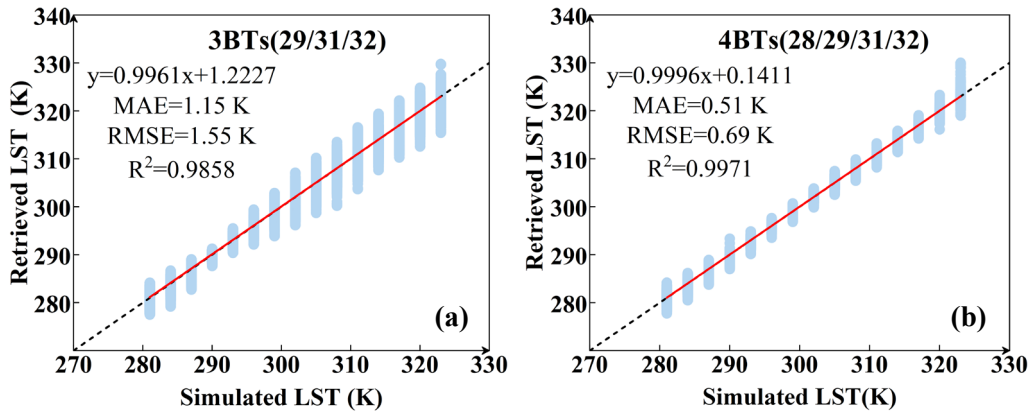
At the same time, we calculated the emission rates, focusing primarily on the emission rate errors for bands 31 and 32 in the 28,29,31,32 band combination. Data from **Table 5-Table 6** indicate that when using the four TIR bands, the retrieval errors for LSE31 and LSE32 are similar, with MAE below 0.01. This demonstrates that this band combination has high accuracy and stability in LSE retrieval. **Fig. 6(d)** shows the distribution histogram of LSE31 and LSE32 retrieval differences, most of which are concentrated near 0. Considering the impact on the accuracy of WVC retrieval, we chose the emissivity from bands 31 and 32 as inputs. We use the retrieved LST and LSE as prior knowledge for WVC retrieval, addressing the issue of insufficient WVC information in satellite data.

Table 5. Band 28-29-31-32 combined retrieval LSE31 error.

Layer \ Node	500		600		700		800		900	
	MAE	RMSE	MAE	RMSE	MAE	RMSE	MAE	RMSE	MAE	RMSE
6	0.005	0.007	0.009	0.023	0.006	0.01	0.01	0.033	0.032	0.222
7	0.006	0.007	0.007	0.036	0.008	0.03	0.007	0.019	0.01	0.049
8	0.008	0.023	0.012	0.074	0.007	0.018	0.007	0.013	0.007	0.027
9	0.008	0.018	0.008	0.017	0.008	0.020	0.008	0.018	0.008	0.02
10	0.008	0.025	0.007	0.013	0.006	0.015	0.007	0.033	0.007	0.02

Table 6. Band 28-29-31-32 combined retrieval LSE32 error.

Layer \ Node	500		600		700		800		900	
	MAE	RMSE	MAE	RMSE	MAE	RMSE	MAE	RMSE	MAE	RMSE
6	0.005	0.008	0.005	0.008	0.01	0.052	0.006	0.015	0.005	0.01
7	0.005	0.006	0.01	0.1	0.004	0.005	0.006	0.019	0.006	0.03
8	0.005	0.008	0.006	0.016	0.005	0.008	0.005	0.01	0.005	0.007
9	0.007	0.035	0.005	0.006	0.006	0.019	0.005	0.012	0.005	0.009
10	0.005	0.006	0.005	0.01	0.007	0.026	0.006	0.027	0.008	0.03



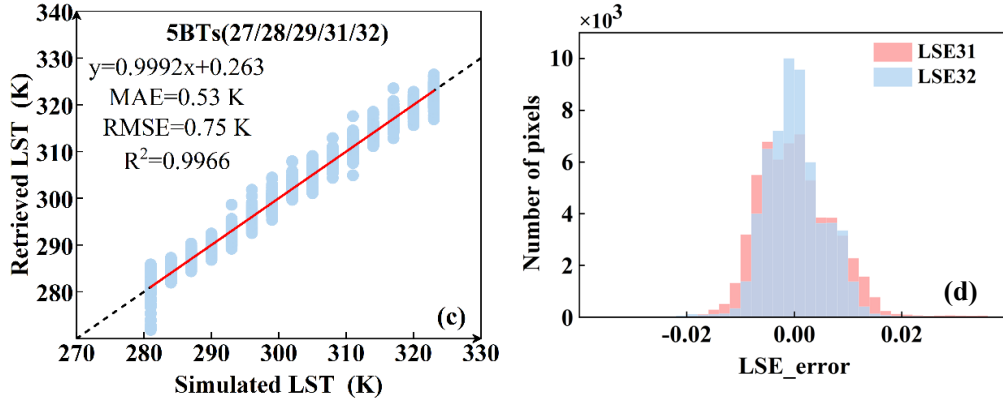


Fig. 6. (a)(b)(c) The scatterplot of LST results is retrieved from different band combination simulation data. (d) Histogram of LSE retrieval difference.

4.1.2 WVC

For the retrieval of WVC, we used the retrieved LST and LSE as prior knowledge and employed a cross-iteration method to solve WVC. The results of DL retrieval with band combinations without prior knowledge are shown in **Table 7-Table 8**, while the errors for band combinations with prior knowledge are summarized in **Table 9-Table 10**. Comparing **Table 7** and **Table 9**, it can be seen that for the 27, 28, 31, and 32 band combination, the highest retrieval accuracy is achieved with 6 hidden layers and 500 nodes per layer, with MAE = 0.06 g/cm² and RMSE = 0.09 g/cm². After incorporating prior knowledge into the retrieval for these four TIR bands, the highest accuracy is achieved with 7 hidden layers and 900 nodes per layer, with MAE = 0.05 g/cm² and RMSE = 0.08 g/cm², as shown in **Table 9**. The incorporation of prior knowledge resulted in only marginal reductions of 0.01 g/cm² in both MAE and RMSE. Comparing **Table 8** and **Table 10**, it can be seen that the retrieval accuracy for WVC did not improve. Based on preliminary analysis, we found that the retrieval results for the four TIR band combination, whether or not incorporating prior knowledge, are similar to those for the five TIR band combination, with only marginal improvement in accuracy after adding prior knowledge. This is because the common bands in the combination, 27 and 28, are water vapor absorption bands, which are less influenced by the ground. On the other hand, LST and LSE, used as prior knowledge, have inherent errors themselves, which may not significantly improve the accuracy when incorporated into WVC retrieval.

Table 7. Band 27,28,31,32 combined retrieval WVC error.

Layer \ Node	500		600		700		800		900	
	MAE	RMSE	MAE	RMSE	MAE	RMSE	MAE	RMSE	MAE	RMSE
6	0.06	0.09	0.09	0.35	0.07	0.23	0.07	0.26	0.08	0.23
7	0.10	0.37	0.06	0.22	0.07	0.23	0.08	0.28	0.07	0.24
8	0.09	0.32	0.07	0.27	0.09	0.37	0.06	0.23	0.09	0.25
9	0.07	0.32	0.08	0.33	0.07	0.31	0.08	0.33	0.06	0.24
10	0.09	0.30	0.10	0.43	0.09	0.24	0.06	0.20	0.06	0.23

Table 8. Band 27,28,29,31,32 combined retrieval WVC error.

Layer	500		600		700		800		900	
Node	MAE	RMSE	MAE	RMSE	MAE	RMSE	MAE	RMSE	MAE	RMSE
6	0.13	0.31	0.12	0.36	0.10	0.24	0.11	0.33	0.09	0.23
7	0.14	0.40	0.10	0.26	0.09	0.30	0.11	0.21	0.10	0.28
8	0.07	0.09	0.17	0.45	0.15	0.38	0.09	0.26	0.09	0.22
9	0.15	0.39	0.13	0.33	0.11	0.26	0.07	0.13	0.07	0.13
10	0.14	0.30	0.09	0.29	0.10	0.21	0.10	0.30	0.09	0.29

Table 9. Band 27,28,31,32+LST+LSE combined retrieval WVC error.

Layer	500		600		700		800		900	
Node	MAE	RMSE	MAE	RMSE	MAE	RMSE	MAE	RMSE	MAE	RMSE
6	0.13	0.29	0.10	0.24	0.08	0.24	0.07	0.18	0.06	0.17
7	0.08	0.21	0.06	0.16	0.08	0.17	0.07	0.13	0.05	0.08
8	0.12	0.19	0.10	0.17	0.07	0.18	0.06	0.08	0.08	0.22
9	0.06	0.13	0.11	0.18	0.09	0.28	0.09	0.21	0.14	0.32
10	0.12	0.20	0.07	0.14	0.09	0.25	0.07	0.15	0.08	0.22

Table 10. Band 27,28,29,31,32+LST+LSE combined retrieval WVC error.

Layer	500		600		700		800		900	
Node	MAE	RMSE	MAE	RMSE	MAE	RMSE	MAE	RMSE	MAE	RMSE
6	0.13	0.26	0.12	0.24	0.11	0.26	0.09	0.14	0.10	0.21
7	0.11	0.17	0.11	0.16	0.15	0.29	0.13	0.29	0.08	0.12
8	0.12	0.28	0.10	0.17	0.08	0.10	0.07	0.12	0.08	0.16
9	0.13	0.25	0.08	0.13	0.08	0.12	0.08	0.12	0.07	0.19
10	0.15	0.25	0.10	0.18	0.13	0.27	0.08	0.12	0.08	0.15

Additionally, we conducted a statistical analysis of the four most accurate error sets from **Table 7-Table 10**. Shown from **Fig. 7** it is clear that the data points of the retrieval results fit well with the simulated data, with a linear regression slope close to 1. However, in the regions of lower and higher WVC, the retrieval errors increase significantly. This is primarily due to the smaller sample size at the beginning and end of the dataset., and the neural network model cannot fully learn the characteristics of these data, resulting in increased retrieval errors. Overall, the retrieval accuracy with prior knowledge is higher than that without prior knowledge. Therefore, when the TIR band combination for WVC retrieval includes enough bands that are sensitive to water vapor, it is not necessary to include LST and LSE as prior knowledge. Only when the band combination is insufficient, meaning the number of bands is less than or equal to three, should high-quality prior knowledge be added to improve the overall retrieval accuracy.

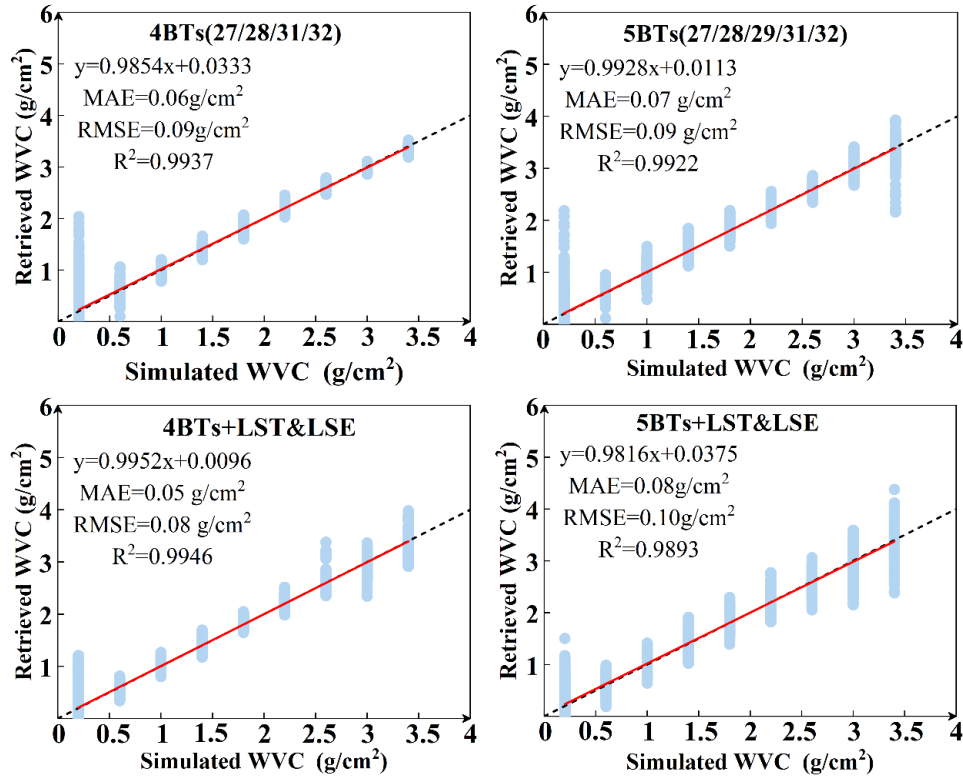


Fig. 7. The scatterplot of WVC results is retrieved from different band combination simulation data.

4.2 Application Analysis and Validation

The study area encompasses the southern region of North America (Fig. 8), spanning longitudes from 65°W to 125°W and latitudes from 10°N to 49°N. The entire region is situated in the northern part of the Western Hemisphere, bordered by the Atlantic Ocean to the east, the Pacific Ocean to the west, and the Gulf of Mexico and the Caribbean Sea to the south. It includes Mexico, the southwestern United States, and the Caribbean islands. The topography is highly diverse, characterized by varied landforms and a general west-high, east-low elevation trend. The climate ranges from arid deserts to humid mountainous zones. Vast plains, dominated by grasslands and croplands, support the region's agricultural economy. This geomorphological diversity provides a unique platform for remote sensing and environmental studies, making the area an ideal location for investigating land surface processes, ecosystem responses, and the impacts of climate change.

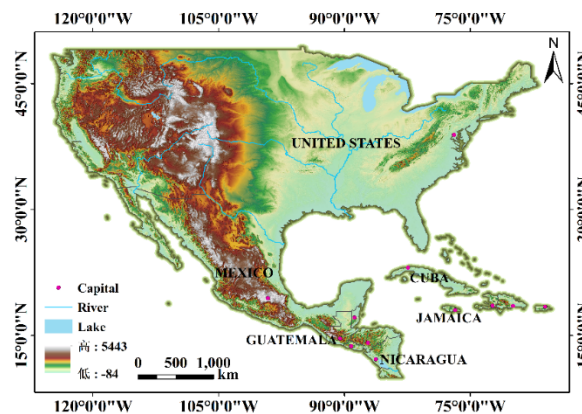


Fig. 8. Study area of southern North America.

4.2.1 Cross verification

(1) LST and LSE

Based on the above logical reasoning and theoretical accuracy verification analysis, it is evident that in LST retrieval, using four thermal infrared bands to form the radiative transfer equation system achieves the highest retrieval accuracy, with RMSE values all below 1 K. Therefore, we employed the multi-parameter joint retrieval method based on AI proposed in this paper to retrieve the LST in the southern region of North America from MODIS product image data. Two MODIS images were selected for the study to validate the application of the aforementioned method, with dates corresponding to daytime on August 2, 2021, and nighttime on August 3, 2021. The BTs of EOS/MODIS products with the best TIR bands is selected as the input parameter, and the output is the LST and LSE respectively.

As shown in **Fig. 9**, the spatial distribution of LST retrieved by the proposed method generally aligns with that of the MODIS land surface temperature product, with white areas indicating invalid/missing values. Across the study region, LST exhibits a gradual increase from the northeast to the southwest, a pattern consistent with the spatial distribution of regional climate zones. According to 10, for daytime LST retrievals, the MAE and RMSE were 0.69 K and 1.49 K respectively, with a Bias of 0.002. Nighttime LST retrievals showed lower errors, with MAE and RMSE values of 0.43 K and 0.72 K respectively, and a Bias of -0.132. The results demonstrate that nighttime LST retrieval achieves higher accuracy than daytime retrieval when using artificial intelligence techniques, primarily due to reduced interference factors such as solar irradiation during nighttime. Furthermore, the differences between MODIS official LST products and our proposed method's retrievals predominantly fall within the range of -1 K to 1 K for both daytime and nighttime observations. **Fig. 11** and **Fig. 12** present comparative results between the LSE spatial distribution patterns retrieved in this study (Bands 31 and 32) and the official MODIS LSE products, demonstrating generally consistent spatial distribution characteristics. As shown in the error distribution maps (**Fig. 13** and **Fig. 14**), the daytime LSE retrieval accuracy for Bands 31 and 32 yielded MAEs of 0.004 and 0.003, respectively, with both RMSEs at 0.006. Nighttime retrievals for both bands showed identical MAEs of 0.004 and RMSEs of 0.005. Comparing **Fig. 13** and **Fig. 14**, it can be seen that the retrieval results of LSE during both day and night maintain high precision and consistency. The difference between MODIS LSE products and retrieved LSE is mostly within -0.01 to 0.01, indicating the robustness of the joint retrieval method for both daytime and nighttime retrievals. It is noteworthy that, when comparing **Fig. 10**, **Fig. 13**, **Fig. 14**, we found that in the southwestern region of the study area, the LST and LSE retrieval results show significant errors. This is due to the fact that the selected data primarily focuses on the summer months, which results in insufficient range and diversity of training data, affecting the performance of the retrieval model under different climatic conditions.

Nevertheless, the proposed retrieval algorithm demonstrates high consistency and reliability in LST and LSE retrievals. This AI-based joint retrieval approach enhances the accuracy of the retrieval results, showing clear advantages. For example, the next step could involve increasing the diversity of training data, including data from different seasons, climatic conditions, and surface types, as well as integrating multi-source remote sensing and ground observation data. This would

enhance the model's generalization capability across various environments, improving its robustness and accuracy in practical applications.

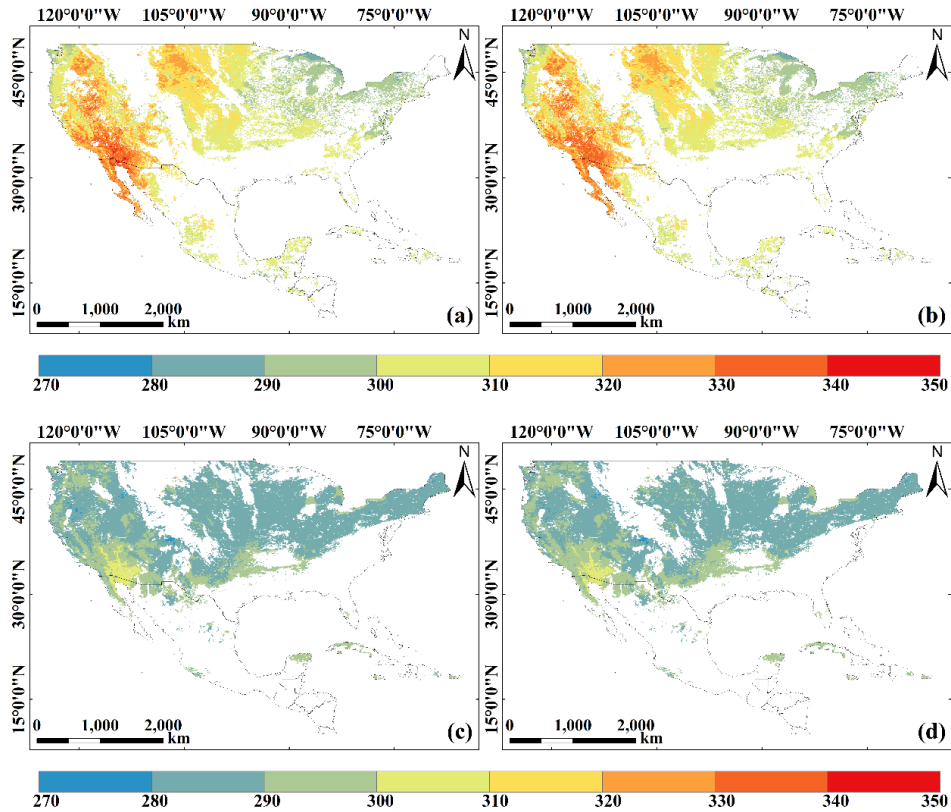


Fig. 9. (a)(c) MODIS LST product images (day and night). (b)(d) LST retrieved from MODIS bands 28,29, 31, 32 (day and night).

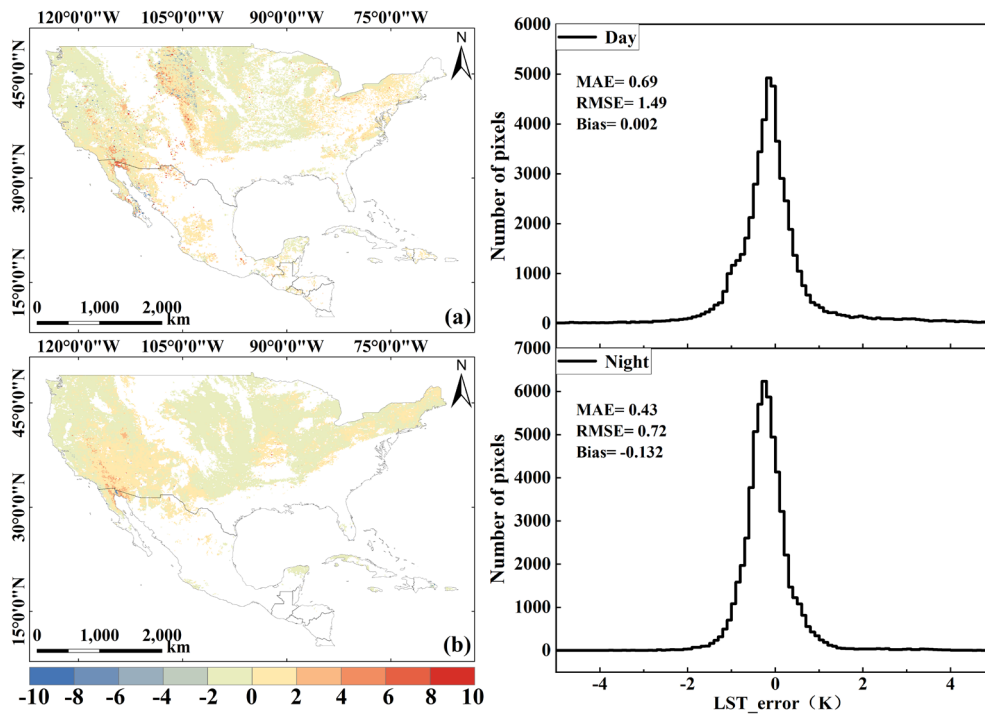


Fig. 10. LST retrieval error analysis combination chart (day and night).

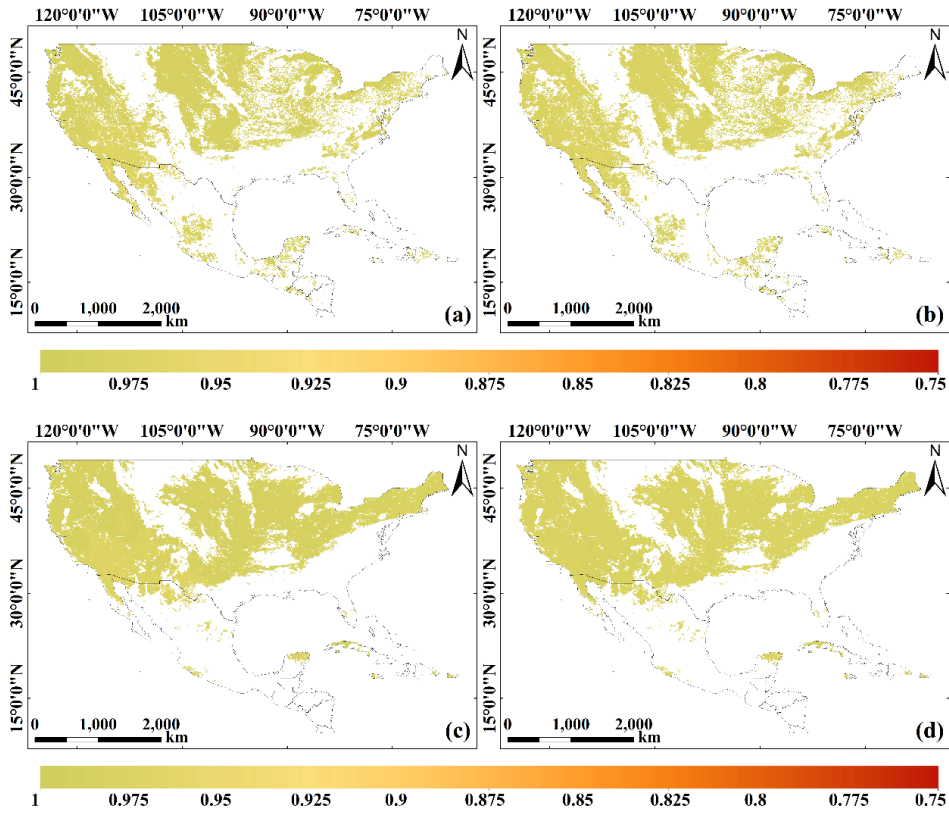


Fig. 11. (a)(c) MODIS LSE31 product images (day and night). (b)(d) LSE31 retrieved from MODIS bands (day and night).

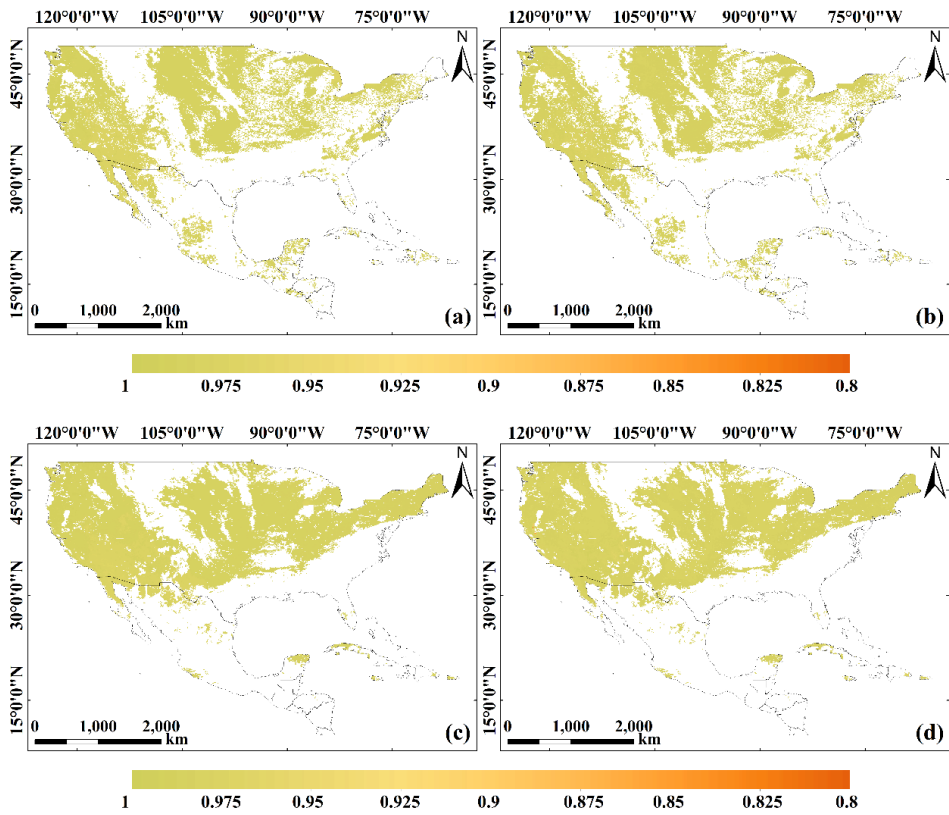


Fig. 12. (a)(c) MODIS LSE32 product images (day and night). (b)(d) LSE32 retrieved from MODIS bands (day and night).

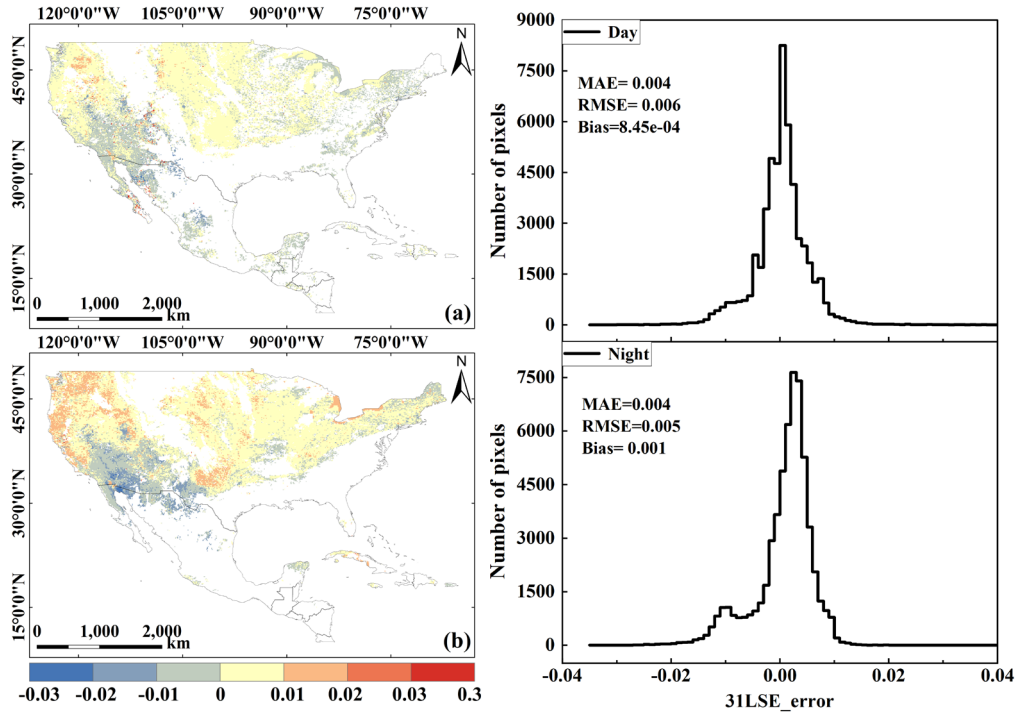


Fig. 13. LSE31 retrieval error analysis combination chart (day and night)

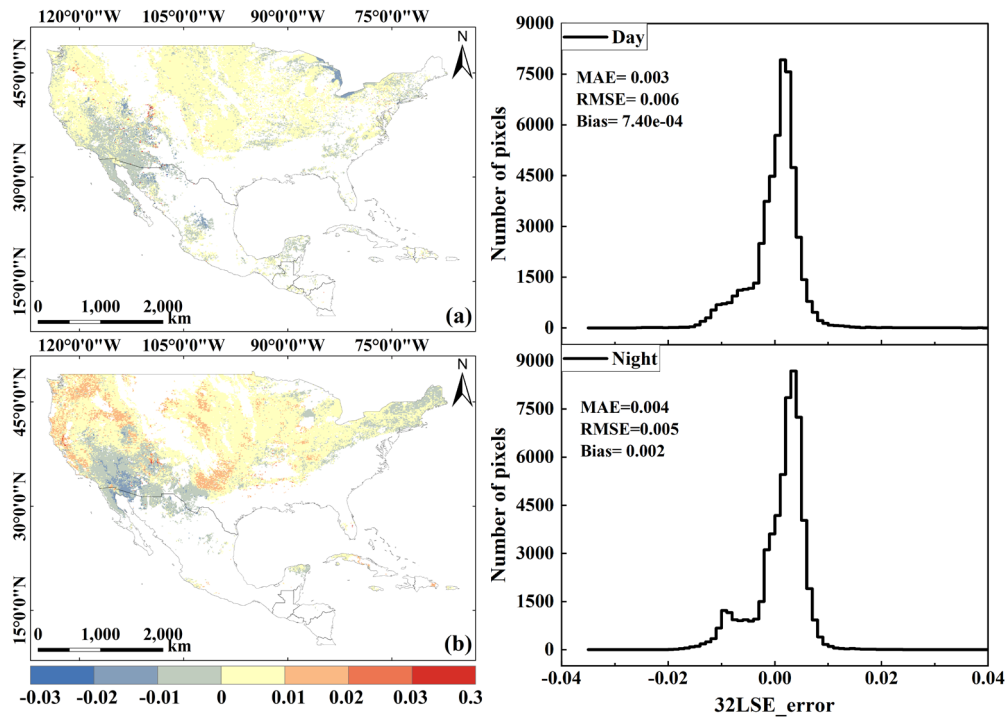


Fig. 14. LSE32 retrieval error analysis combination chart (day and night)

(2) WVC

Based on the theoretical accuracy analysis and validation of WVC, this study uses MODIS WVC product images from August 2, 2021 (day) and August 3, 2021 (night) to evaluate the proposed method. MODIS offers two types of WVC algorithms: a visible and near-infrared algorithm for daytime and a thermal infrared algorithm suitable for both day and night. This study utilizes the

thermal infrared WVC product images for both periods. The validation was conducted using the optimal band combination, with BT values, along with the retrieved LST and LSE as input parameters, and WVC as the output.

Fig. 15(a)(c) show the spatial distribution of MODIS products using thermal infrared algorithms, while **Fig. 15(b)(d)** display the WVC (day and night) retrieved using the proposed method in this paper, with white areas indicating invalid values. The spatial distribution trends of the two are relatively consistent. The spatial distribution characteristics of differences between MODIS WVC products and our retrieved WVC are presented in **Fig. 16**. Under daytime conditions, the atmospheric water vapor content retrievals yielded MAE and RMSE values of 0.56 g/cm^2 and 0.93 g/cm^2 , respectively. Nighttime WVC retrievals demonstrated improved accuracy, with corresponding MAE and RMSE values of 0.47 g/cm^2 and 0.63 g/cm^2 . Statistical results indicate that the differences between retrieved and reference WVC values are predominantly distributed within the range of -1 g/cm^2 to 1 g/cm^2 for both daytime and nighttime conditions. Notably, nighttime WVC differences show stronger concentration around 0 g/cm^2 compared to daytime retrievals. This improved nighttime consistency likely results from reduced thermal radiation effects on atmospheric water vapor during nighttime conditions, leading to more stable model performance and higher agreement with MODIS WVC products. Consequently, further model optimization and data processing may enhance the accuracy of daytime WVC retrievals.

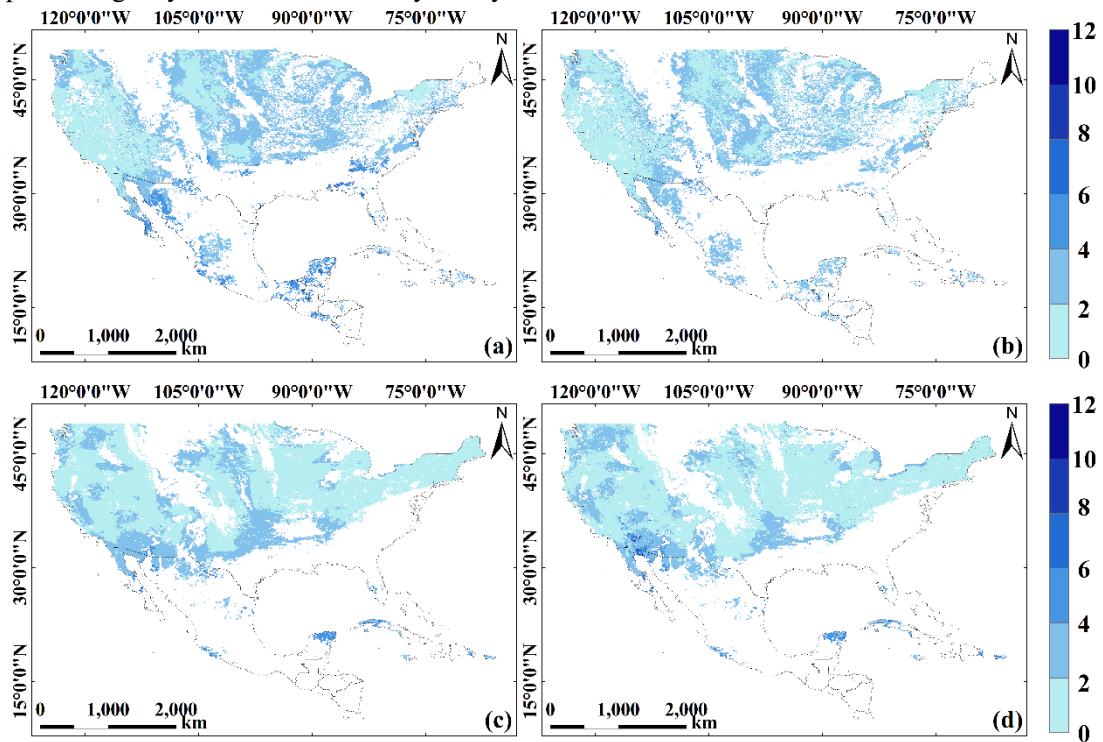


Fig. 15. (a)(c) MODIS WVC product images (day and night). (b)(d) WVC retrieved from MODIS bands (day and night).

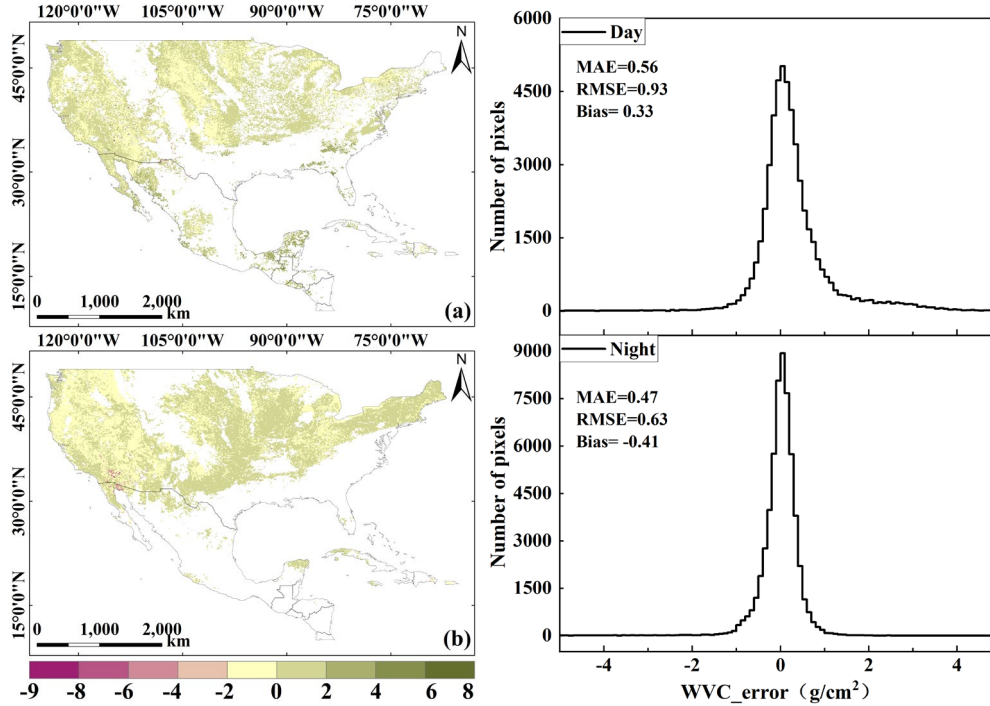


Fig. 16. WVC retrieval error analysis composite map (day and night)

4.3 Ground Data Validation

Ground data analysis is crucial for validating the accuracy and reliability of the joint retrieval algorithm, with the availability and quality of data significantly impacting the verification process (Wang et al., 2024). Given the limited number of observation stations related to LSE and the difficulty in obtaining such data, this study primarily focuses on validating the jointly retrieved LST and WVC by comparing the retrieval values with the measurements from ground observation stations to assess their performance and practicality.

Fig. 17(a)(b) show the scatter plots verified by LST ground monitoring during the day and night respectively. Under daytime conditions, the MAE and RMSE of LST retrieval were 1.47 K and 1.80 K, respectively, while during nighttime, the MAE and RMSE were 1.28 K and 1.63 K, indicating higher retrieval accuracy at night. This phenomenon occurs because, during the day, solar radiation causes rapid and uneven changes in LST, leading to larger retrieval errors. Additionally, factors such as atmospheric humidity, aerosols, and surface albedo, which can affect retrieval accuracy, are relatively stable at night. At night, the LST changes are smaller, and there is less atmospheric disturbance, reflecting more stable radiative transfer conditions. This leads to retrieval results that are closer to the actual conditions. The "4BTs+LST&E" band combination was selected for WVC ground observation station retrieval validation during the daytime. As shown in Fig. 17c, only the scatter plot of daytime WVC station observation validation is presented, with MAE and RMSE values of 0.31 g/cm² and 0.38 g/cm², respectively, and an R² value of 0.83. The validation results from the ground-based observation site for the AI-based joint retrieval algorithm of LST, LSE, and WVC, combined with the aforementioned simulation and cross-validation results, consistently demonstrate that the proposed joint retrieval algorithm achieves high accuracy and reliability, providing a solid foundation for its further application and promotion.

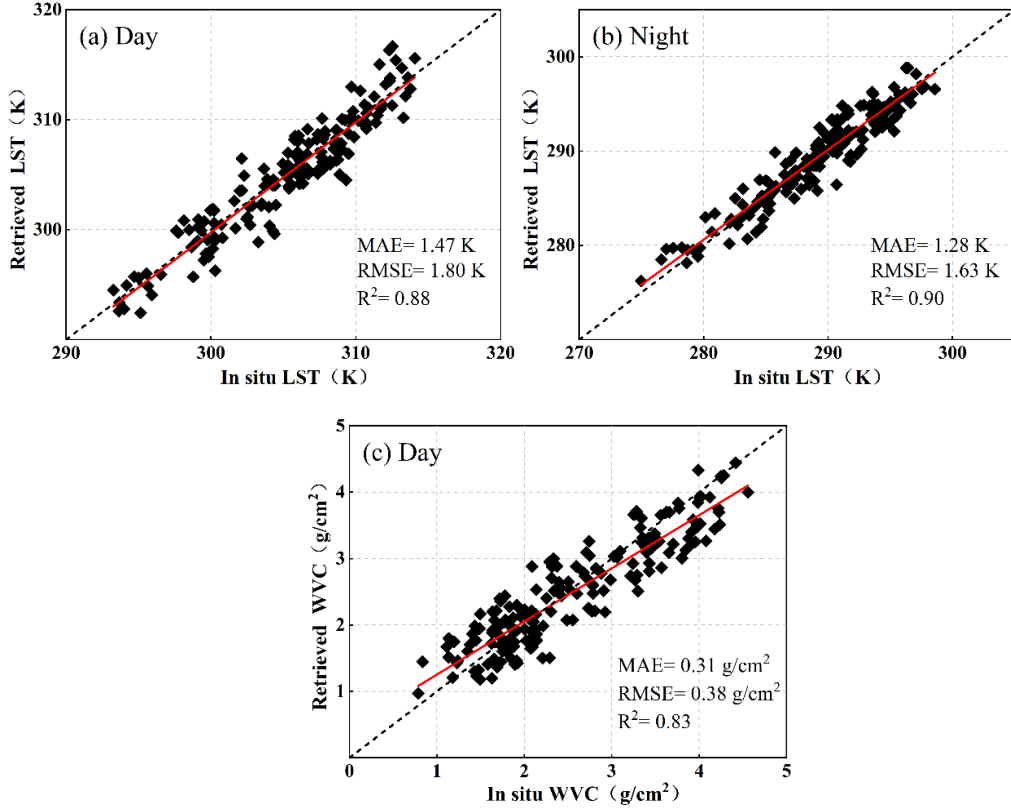


Fig. 17. (a)(b) Scatter plot of ground validation data for LST retrieval (day and night). (c) Scatter plot of ground validation data for WVC retrieval (day)

5. Conclusion

Changes in LST, LSE, and WVC have significant impacts not only on the Earth's climate system and energy balance but also on human life, production, economy, and social development. This paper proposes a method based on AI technology that couples physical and statistical methods to jointly retrieve LST, LSE, and WVC from thermal infrared remote sensing data. Based on radiative transfer theory, deep learning can establish causal relationships between input parameters and output parameters, enabling the construction of a complete set of closed equations. It is noteworthy that physical simulation data alone cannot describe all scenarios. Therefore, a generalized statistical method is constructed to supplement the real situation with multi-source data, mainly for mixed pixel cases. The results show that this algorithm is not only theoretically feasible but also practically viable, achieving improved retrieval accuracy.

In this study, considering the design of the sensor's spectral bands, different band combinations were constructed and used for scenario retrievals during both daytime and nighttime. First, the numerical experiment results from radiative transfer simulation indicated that when using four TIR bands, RMSE of LST retrieval was less than 1K, and the retrieval errors for LES31 and LES32 were similarly low, both below 0.01. By combining four TIR bands with LST and emissivity information, the accuracy of WVC retrieval was significantly improved through cross-iteration, eliminating uncertainties and resulting in stable WVC retrievals with an RMSE of approximately 0.09 g/cm². The algorithm for retrieving LST, LSE, and WVC in the southern region of North America was validated through cross-validation and evaluation using data from ground observation stations, yielding consistent results. Despite certain limitations, all three validation methods led to similar

conclusions, demonstrating that the AI-based approach, which combines physical and statistical methods, effectively addresses the shortcomings of traditional retrieval methods. It accurately retrieves geophysical parameters while offering a physically interpretable solution for deep learning in retrieval.

Authors contribution

All the authors make substantial contribution in this manuscript. **Liurui Xiao**: validation, formal analysis, research, resources, data organization, writing. **Kebiao Mao**: Financial support, Conceptualization, Methodology, Review and editing. **Chunshu Li**: validation, formal analysis, review and editing. **Jiancheng shi, Sayed M, Bateni and Wang Dai**: review and editing, supervision. all the authors discussed the results and implication on the manuscript at all stages.

Declaration of Competing interest

The authors declare that they have no known competing financial interests or personal relationships that could have appeared to influence the work reported in this paper.

Acknowledgments

This research was supported by the National Key R&D Program of China under grant number 2023YFB3906202, for which we are profoundly grateful. We also extend our sincere thanks to the anonymous reviewers and the editor for their valuable comments and suggestions on this paper. The MODIS thermal infrared data used in this study were provided by the National Aeronautics and Space Administration (NASA), and we extend our gratitude for their support. We also appreciate the Surface Radiation Budget Network (SURFRAD) ground observation data provided by the National Oceanic and Atmospheric Administration (NOAA), the AERONET ground observation data provided by NASA and the French National Center for Scientific Research (CNRS), and the ERA5 reanalysis data provided by the European Centre for Medium-Range Weather Forecasts (ECMWF). These high-quality datasets were crucial to the successful completion of this research.

References

- Anderson, M.C., Kustas, W.P., Norman, J.M., 2003. Upscaling and downscaling—A regional view of the soil–plant–atmosphere continuum. *Agronomy Journal*. 95(6), 1408–1423. <https://doi.org/10.2134/agronj2003.1408>.
- Akkem, Y., Biswas, S. K., Varanasi, A. 2023. Smart farming using artificial intelligence: A review. *Engineering Applications of Artificial Intelligence*, 120, 105899. <https://doi.org/10.1016/j.engappai.2023.105899>.
- Bai, J.N., Lou, Y.D., Zhang, W.X., et al., 2021. Assessment and calibration of MODIS precipitable water vapor products based on GPS network over China. *Atmospheric Research*. 254, 105504–105514. <https://doi.org/10.1016/j.atmosres.2021.105504>.
- Becker, F., LI, Z-L., 1990. Towards a local split window method over land surfaces. *International Journal of Remote Sensing*. 11(3), 369–393. <https://doi.org/10.1080/01431169008955028>.

- Cristobal, J., Jimenez - Muñoz, J.C., Sobrino, J.A., Ninyerola, M., Pons, X., 2009. Improvements in land surface temperature retrieval from the Landsat series thermal band using water vapor and air temperature. *Journal of Geophysical Research: Atmospheres*. 114(D8). <https://doi.org/10.1029/2008JD010616>.
- Dalu, G., 1986. Satellite remote sensing of atmospheric water vapor. *International Journal of Remote Sensing*. 7(9), 1089-1097. <https://doi.org/10.1080/01431168608948911>.
- Franc, G.B., Cracknell, A.P., 1994. Retrieval of land and sea surface temperature using NOAA-11 AVHRR data in north-eastern Brazil. *International Journal of Remote Sensing*. 15(8), 1695-1712. <https://doi.org/10.1080/01431169408954201>.
- Frantz, D., Stellmes, M., Hostert, P., 2019. A Global MODIS Water Vapor Database for the Operational Atmospheric Correction of Historic and Recent Landsat Imagery. *Remote Sensing*. 11(3), 257. <https://doi.org/10.3390/rs11030257>.
- Gao B C, Kaufman Y J. Water vapor retrievals using Moderate Resolution Imaging Spectroradiometer (MODIS) near-infrared channels[J]. *Journal of Geophysical Research: Atmospheres*, 2003, 108(D13). <https://doi.org/10.1029/2002JD003023>.
- Gillespie, A., Rokugawa, S., Matsunaga, T., Cothorn, J.S., Hook S and Kahle A.B., 1998. A temperature and emissivity separation algorithm for Advanced Spaceborne Thermal Emission and Reflection Radiometer (ASTER) images. *IEEE Transactions on Geoscience and Remote Sensing*. 36(4), 1113-1126. <https://doi.org/10.1109/36.700995>.
- Hornik, K., Stinchcombe, M., & White, H., 1989. Multilayer feedforward networks are universal approximators. *Neural networks*, 2(5), 359-366. [https://doi.org/10.1016/0893-6080\(89\)90020-8](https://doi.org/10.1016/0893-6080(89)90020-8).
- Huang, P., Guo, Q., Han, C., et al., 2021. An Improved Method Combining ANN and 1D-Var for the Retrieval of Atmospheric Temperature Profiles from FY-4A/GIIRS Hyperspectral Data. *Remote Sensing*. 13(3), 481. <https://doi.org/10.3390/rs13030481>.
- Jha, K., Doshi, A., Patel, P., Shah, M., 2019. A comprehensive review on automation in agriculture using artificial intelligence. *Artificial Intelligence in Agriculture*, 2, 1-12. <https://doi.org/10.1016/j.aiia.2019.05.004>.
- Jiménez-Muñoz, J.C., Sobrino, J.A., Ninyerola, M., Pons, X., 2003. A generalized single-channel method for retrieving land surface temperature from remote sensing data. *Journal of Geophysical Research Atmospheres*. 108(D22), 4688. <https://doi.org/10.1029/2003JD003480>.
- Lan, X.Y., Zhao, E.Y., Leng, P., Li, Z.L., Labed J, Nerry F, Zhang, X., Shang, G.F., 2021. Alternative physical method for retrieving land surface temperatures from hyperspectral thermal infrared data: Application to IASI observations. *IEEE Transactions on Geoscience and Remote Sensing*. 60, 1-12. <https://doi.org/10.1109/TGRS.2021.3056103>.
- Li, J., Hong, D., Gao, L., Yao, J., Zheng, K., Zhang, B., Chanussot, J., 2022. Deep learning in multimodal remote sensing data fusion: A comprehensive review. *International Journal of Applied Earth Observation and Geoinformation*, 112, 102926. <https://doi.org/10.1016/j.jag.2022.102926>.
- Mao, K., Shi, J., Li, Z. L., Tang, H., 2007. An RM - NN algorithm for retrieving land surface temperature and emissivity from EOS/MODIS data. *Journal of geophysical research: Atmospheres*, 112(D21102). <https://doi.org/10.1029/2007JD008428>.
- Mao, K., Shi, J., Tang, H., Li, Z. L., Wang, X., & Chen, K. S., 2008. A neural network technique for separating land surface emissivity and temperature from ASTER imagery. *IEEE Transactions on Geoscience and Remote Sensing*, 46(1), 200-208. <https://doi.org/10.1109/TGRS.2007.907333>.
- Mao, K., Li, S., Wang, D., Zhang, L., Wang, X., Tang, H., Li, Z. L. 2011. Retrieval of land surface temperature and emissivity from ASTER1B data using a dynamic learning neural network. *International journal of remote sensing*, 32(19), 5413-5423. <https://doi.org/10.1080/01431161.2010.501043>.

- Mao, K., Wang, H., Shi, J., Heggy, E., Wu, S., Bateni, S. M., Du, G. 2023a. A general paradigm for retrieving soil moisture and surface temperature from passive microwave remote sensing data based on artificial intelligence. *Remote sensing*, 15(7), 1793. <https://doi.org/10.3390/rs15071793>.
- Mao, K.B., Zhang, C.Y., Shi, J.C., Wang, X.M., Guo, Z.H., Li, C.S., Dong, L.X., 2023b. The Paradigm Theory and Judgment Conditions of Geophysical Parameter Retrieval Based on Artificial Intelligence. *Smart Agriculture*. 5(2), 161-171. <https://doi.org/10.12133/j.smartag.SA202304013>.
- McMillin, L.M., 1975. Estimation of sea surface temperatures from two infrared window measurements with different absorption. *Journal of geophysical research*. 80(36), 5113-5117. <https://doi.org/10.1029/JC080i036p05113>.
- Mikhaylov, A., Moiseev, N., Aleshin, K., Burkhardt, T., 2020. Global climate change and greenhouse effect. *Entrepreneurship and Sustainability Issues*. 7(4), 2897-2913. [https://doi.org/10.9770/jesi.2020.7.4\(21\)](https://doi.org/10.9770/jesi.2020.7.4(21)).
- Moisa**, M. B., Gabissa, B. T., Hinkosa, L. B., Dejene, I. N., Gemedo, D. O., 2022. Analysis of land surface temperature using geospatial technologies in Gida Kiremu, Limu, and Amuru District, Western Ethiopia. *Artificial Intelligence in Agriculture*, 6, 90-99. <https://doi.org/10.1016/j.aiia.2022.06.002>.
- Ndossi, M.I., Avdan, U., 2016. Inversion of land surface temperature (LST) using Terra ASTER data: a comparison of three algorithms. *Remote Sensing*. 8(12), 993. <https://doi.org/10.3390/rs8120993>.
- Nie, J., Ren, H.Z., Zheng, Y.T., Ghent D and Tansey K., 2021. Land surface temperature and emissivity retrieval from nighttime middle infrared and thermal-infrared Sentinel-3 images. *IEEE Geoscience and Remote Sensing Letters*. 18(5), 915-919. <https://doi.org/10.1109/lgrs.2020.2986326>.
- Padmanabhan, S., Reising, S.C., Vivekanandan, J., Iturbide-Sanchez F., 2009. Retrieval of atmospheric water vapor density with fine spatial resolution using three-dimensional tomographic inversion of microwave brightness temperatures measured by a network of scanning compact radiometers. *IEEE Transactions on Geoscience and Remote Sensing*. 47(11), 3708-3721. <https://doi.org/10.1109/TGRS.2009.2031107>.
- Price, J.C., 1984. Land surface temperature measurements from the split window channels of the NOAA 7 Advanced Very High-Resolution Radiometer. *Journal of Geophysical Research: Atmospheres*. 89(D5), 7231-7237. <https://doi.org/10.1029/jd089id05p07231>.
- Qin, Z.H., Karnieli, A., Berliner, P., 2001a. A mono-window algorithm for retrieving land surface temperature from Landsat TM data and its application to the Israel-Egypt border region. *International Journal of Remote Sensing*. 22 (18), 3719-3746. <https://doi.org/10.1080/01431160010006971>.
- Qin, Z., Dall'Olmo, G., Karnieli, A., Berliner, P., 2001b. Derivation of split window algorithm and its sensitivity analysis for retrieving land surface temperature from NOAA - advanced very high resolution radiometer data. *Journal of Geophysical Research: Atmospheres* (1984–2012), 106, 22655-22670. <https://doi.org/10.1029/2000JD900452>.
- Raynolds, M.K., Comiso, J.C., Walker, D.A., Verbyla, D., 2008. Relationship between Satellite-derived Land Surface Temperatures Arctic Vegetation Types, and NDVI. *Remote Sensing of Environment*. 112(19), 1884-1894. <https://doi.org/10.1016/j.rse.2007.09.008>.
- Seemann, S.W., Li, J., Menzel, W.P., et al., 2003. Operational retrieval of atmospheric temperature, moisture, and ozone from MODIS infrared radiances. *Journal of Applied Meteorology*. 42(8), 1072-1091. [https://doi.org/10.1175/1520-0450\(2003\)042<1072:OROATM>2.0.CO;2](https://doi.org/10.1175/1520-0450(2003)042<1072:OROATM>2.0.CO;2).
- Seguin, B., Becker, F., Phulpin, T., Gu, X., Guyot, G., Kerr, Y., King, C., Lagouarde, J., Ottle' C, Stoll, M., Tabbagh, T., Vidal A., 1999. IRSUTE: a minisatellite project for land surface heat flux estimation from field to regional scale. *Remote Sensing of Environment*. 68(3), 357-369. [https://doi.org/10.1016/S0034-4257\(98\)00122-9](https://doi.org/10.1016/S0034-4257(98)00122-9).

- Snyder, W.C., Wan, Z., Zhang, Y., Feng, Y.Z., 1998. Classification-based emissivity for land surface temperature measurement from space. *International Journal of Remote Sensing*. 19(14), 2753-2774. <https://doi.org/10.1080/014311698214497>.
- Sobrino, J.A., Raissouni, N., Simarro, J., Nerry, F., Petitcolin, F., 1999. Atmospheric water vapor content over land surfaces derived from the AVHRR data: Application to the Iberian Peninsula. *IEEE Transactions on Geoscience and Remote Sensing*. 37(3), 1425-1434. <https://doi.org/10.1109/36.763306>.
- Toporov, M., Löhnert, U., 2020. Synergy of satellite-and ground-based observations for continuous monitoring of atmospheric stability, liquid water path, and integrated water vapor: Theoretical evaluations using reanalysis and neural networks. *Journal of Applied Meteorology and Climatology*. 59(7), 1153-1170. <https://doi.org/10.1175/JAMC-D-19-0169.1>.
- Tu, J., Lu, E., 2020. Relative importance of water vapor and air temperature in the interannual variation of the seasonal precipitation: a comparison of the physical and statistical methods. *Climate Dynamics*. 54(7), 3655-3670. <https://doi.org/10.1007/s00382-020-05197-3>.
- Wan, Z.M., Dozier, J., 1996. A generalized split-window algorithm for retrieving land-surface temperature from space. *IEEE Transactions on Geoscience and Remote Sensing*. 34(4), 892-905. <https://doi.org/10.1109/36.508406>.
- Wan, Z.M, Li, Z., 1997. A physics-based algorithm for retrieving land-surface emissivity and temperature from EOS/MODIS data. *IEEE Transactions on Geoscience and Remote Sensing*. 35(4), 980-996. <https://doi.org/10.1109/36.602541>.
- Wan, Z., Zhang, Y., Zhang, Q., Li, Z.L., 2004. Quality assessment and validation of the MODIS global land surface temperature. *International journal of remote sensing*. 25(1), 261-274. <https://doi.org/10.1080/0143116031000116417>.
- Wan, Z.M., Li, Z.L., 2008. Radiance-based validation of the V5 MODIS land-surface temperature product. *International Journal of Remote Sensing*. 29(17/18), 5373-5395. <https://doi.org/10.1080/01431160802036565>.
- Wan, Z. M. 2014. New refinements and validation of the collection-6 MODIS land-surface temperature/emissivity product. *Remote Sensing of Environment*, 140, 36-45. <https://doi.org/10.1016/j.rse.2013.08.027>.
- Wang, H., Mao, K., Yuan, Z., Shi, J., Cao, M., Qin, Z., Tang, B., 2021. A method for land surface temperature retrieval based on model-data-knowledge-driven and deep learning. *Remote Sensing of Environment*. 265, 112665-112684. <https://doi.org/10.1016/j.rse.2021.112665>.
- Wang, H., Mao, K., Shi, J., Bateni, S. M., Altantuya, D., Sainbuyan, B., Bao, Y., 2024. A normal form for synchronous land surface temperature and emissivity retrieval using deep learning coupled physical and statistical methods. *International Journal of Applied Earth Observation and Geoinformation*, 127, 103704. <https://doi.org/10.1016/j.jag.2024.103704>.
- Wang, R., Liu, Y., 2020. Recent declines in global water vapor from MODIS products: Artifact or real trend. *Remote Sensing of Environment*. 247, 111896. <https://doi.org/10.1016/j.rse.2020.111896>.
- Yin C L, Meng F and Yu Q R. 2020. Calculation of land surface emissivity and retrieval of land surface temperature based on a spectral mixing model. *Infrared Physics and Technology*, 108, 103333. <https://doi.org/10.1016/j.infrared.2020.103333>.
- Zhang, B., Yao, Y., 2021. Precipitable water vapor fusion based on a generalized regression neural network. *Journal of geodesy*, 95(3), 36. <https://doi.org/10.1007/s00190-021-01482-z>.
- Zhang, Y.L., Cai, C.S., Chen, B.Y., et al., 2019. Consistency evaluation of precipitable water vapor derived from ERA5, ERA - Interim, GNSS, and radiosondes over China. *Radio Science*. 54(7), 561-571. <https://doi.org/10.1029/2018RS006789>.